Development and application of an uncapped mRNA platform

Biao Liu[1,6], Peng Ni[3,6], Linkang Cai[3,6], Xiaotai Shi[3,6], Shuaijie Ji[2,6], Zonghuang Ke[3,6], Siqi Zhang[3,6], Bing Hu[4,6], Binfeng Yang[3,6], Yiyan Xu[1], Wei Long[3], Zhizheng Fang[3], Han Hu[1], Yang Wang[1], Wen Zhang[5], Hui Geng[2], Yan. Xu[3], Xiaodi Zheng[1], Zhong Wang[3], Baoqian Zhang[2], Kai Pan[4], Kangping Zhou[4], Yanfang Cui[2], Hanming Wang[3], and Binlei Liu[1,3]

[1] National "111" Center for Cellular Regulation and Molecular Pharmaceutics, Key Laboratory of Fermentation Engineering (Ministry of Education), Hubei Provincial Cooperative Innovation Center of Industrial Fermentation, College of Bioengineering, Hubei University of Technology, Wuhan 430068, P. R. China

[2] Huazhong Normal University, Wuhan 430079, P. R. China

[3] Wuhan Binhui Biopharmaceutical Co., Ltd. Wuhan 430068, P. R. China

[4] Hubei Provincial Centre for Disease Control and Prevention, Wuhan 430068, P. R. China

[5] Department of Immunology, National Cancer Center/National Clinical Research Center for Cancer/Cancer Hospital, Chinese Academy of Medical Sciences and Peking Union Medical College, Beijing 100021, P. R. China

[6] These authors contributed equally: Biao Liu, Peng Ni, Linkang Cai, Xiaotai Shi, Shuaijie Ji, Zonghuang Ke, Siqi Zhang, Bing Hu, Binfeng Yang.

e-mail: yfcui@mail.ccnu.edu.cn, hanming.wang@binhui-bio.com, liubl@hbut.edu.cn

A novel uncapped mRNA platform was developed. Five lipid nanoparticle (LNP)-encapsulated mRNA constructs were made to evaluate several aspects of our platform, including transfection efficiency and durability *in vitro* and *in vivo* and the activation of humoral and cellular immunity in several animal models. The constructs were eGFP-mRNA-LNP (for enhanced green fluorescence mRNA), Fluc-mRNA-LNP

(for firefly luciferase mRNA), $S^{\delta T}$-mRNA-LNP (for Delta strain SARS-CoV-2 spike protein trimer mRNA), gD^{ED}-mRNA-LNP (for truncated glycoprotein D mRNA coding ectodomain from herpes simplex virus type 2 (HSV2)) and gD^{FR}-mRNA-LNP (for truncated HSV2 glycoprotein D mRNA coding amino acids 1~400). Quantifiable target protein expression was achieved *in vitro* and *in vivo* with eGFP- and Fluc-mRNA-LNP. $S^{\delta T}$-mRNA-LNP, gD^{ED}-mRNA-LNP and gD^{FR}-mRNA-LNP induced both humoral and cellular immune responses comparable to those obtained by previously reported capped mRNA-LNP constructs. Notably, 25, 50 and 100 μg of $S^{\delta T}$-mRNA-LNP all elicited neutralizing antibodies in hamsters against the Omicron and Delta strains. Additionally, gD^{ED}-mRNA-LNP and gD^{FR}-mRNA-LNP induced potent neutralizing antibodies in rabbits and mice. The mRNA constructs with uridine triphosphate (UTP) outperformed those with N1-methylpseudouridine triphosphate (N1mψTP) in the *in vivo* expression of luciferase and the induction of antibodies via $S^{\delta T}$-mRNA-LNP. Our uncapped, process-simplified, and economical mRNA platform may have broad utility in vaccines and protein replacement drugs.

Messenger RNA (mRNA) is responsible for transcribing the genetic information stored in DNA and directing the synthesis of proteins in cells. In theory, once transcribed and delivered into the cytoplasm, mRNA can be translated to generate any protein desired. Various problems must be addressed to work with mRNA, such as extreme instability, degradation by RNases that occur widely *in vivo* and *in vitro*[1], dependency on the translation mechanism in the target cells[2], and the propensity to trigger unnecessary immune responses[3]. Efforts have been made for decades to obtain mRNA molecules with strong stability, high translation efficiency, and low immunogenicity. The successful development of the new coronavirus mRNA vaccines indicates that mRNA technology has matured and can be used as a powerful, versatile, and fast-response application platform[4].

Studies have found that many naturally existing mRNA chemical modifications have biological significance in mRNA stability. At present, the following chemical modifications are commonly used in mRNA technology: N1- and N6-methyladenosine (m1A, m6A,

m6Am)[5], 3- and 5-methylcytosine (m3C, m5C)[6], 5-hydroxymethylcytosine (hm5C)[7, 8], 2'-O-methylation (Nm)[9, 10], and pseudouridine (Ψ)[5, 11]. Among them, the methyl group on m1A blocks Watson-Crick base pairing, thereby changing the mRNA structure and promoting translation initiation[12]; m6A is a reversible dynamic RNA modification, an indispensable part of RNA metabolism regulation, which can regulate mRNA stability, splicing, transport, localization, and translation[13-15]; m5C affects mRNA structural stability and translation efficiency and can promote mRNA nuclear export[16-18]; Nm is a cotranscriptional or posttranscriptional modification of mRNA, which can increase the hydrophobicity of mRNA, protect it from nuclease attack, stabilize the helical structure of mRNA, and affect the interaction of mRNA with proteins or other RNAs[19-23]; Ψ is the first and most common mRNA modification discovered[24]. Katalin Karikó et al. have successively found that the introduction of pseudouridine triphosphate (ψTP) into mRNA can reduce its immunogenicity, which decreases with the increase in the proportion of ψTP introduced[25]. Completely replacing uridine triphosphate (UTP) with ψTP mRNA can not only greatly reduce the immunogenicity of mRNA but also improve the stability of mRNA and enhance its translation efficiency[26]. In 2015, Oliwia Andries et al. found that the complete replacement of UTP with N1-methylpseudouridine triphosphate (N1mψTP) reduced the immunogenicity of mRNA and enhanced protein expression more than the complete replacement of UTP with ψTP[27]. The two new coronavirus mRNA vaccines, mRNA-1273 (Moderna, https://www.modernatx.com/research/product-pipeline) and BNT162b2 (Pfizer-BioNTech, https://biontech.de/science/pipeline), both use N1mψTP instead of UTP[28].

To reduce the immunogenicity of mRNA and improve its intracellular stability and translation efficiency, mRNA structures have been designed sequentially to have a 5' cap, a 5'-untranslated region (UTR), a coding region, a 3'-UTR and a polyadenosine tail (poly A or pA). Among them, the poly A tail length[29, 30] and 3'-UTR[31, 32] are critical for mRNA stability. The 5'-UTR is another crucial element that recruits ribosomes and cap-dependent (or cap-independent) regulators to initiate translation. Cap-dependent structures can use analogs, such as m7GpppG, as a protective structure that shields RNA from exonuclease cleavage and initiates mRNA translation[32]. In addition, the internal ribosome entry site (IRES) of some

mRNAs has a similar function to the cap structure. In 1988, Pelletier et al. found that the 5'-UTR of poliovirus has a P2 sequence of approximately 450 nucleotides that can guide eukaryotic mRNA translation[33]; Jang *et al.* also found a sequence in the 5'-UTR of encephalomyocarditis virus[34]. In 1991, Macejak *et al.* found that there is an IRES element in the 5'-UTR of the cellular immunoglobulin heavy chain binding protein gene[35]. Using a constructed circular mRNA, it was demonstrated that IRES can guide protein synthesis *in vitro*, indicating that protein translation can specifically depend on the IRES sequence[36]. IRES facilitates ribosome assembly and initiates translation by recruiting different trans-acting factors, making it possible for protein translation initiation to occur independently of the 5' cap structure of the mRNA.

Complementary to a working mRNA technology is a proper delivery technology. Since the mRNA chain is a negatively charged long-chain macromolecule and the surface of the cell membrane is also negatively charged, electrostatic repulsion makes it difficult for the mRNA molecule to pass through the cell membrane and enter the cell. In addition, mRNA is a single-chain molecule that is very unstable. Once mRNA enters the body, it can be quickly degraded by a variety of enzymes. Therefore, the delivery of mRNA to the interior of cells requires addressing enzymatic degradation and membrane barriers caused by electrostatic repulsion. With the approval of two mRNA vaccines, LNPs are recognized as the most successful mRNA delivery vehicles[37]. Liposomes are vesicle structures composed of lipid molecules that were discovered by scientists A. D. Bangham and R. W. Horne under a microscope as early as 1961[38, 39]. In 1995, the first liposomal drug Doxil approved by the FDA in the US was used for ovarian cancer and breast cancer chemotherapy through the HSPC/DMG-PEG dual component liposome encapsulated drug doxorubicin to reduce the toxicity of free drugs to other organs[40]. In 2018, the U.S. FDA approved Onpattro, a drug that encapsulates nucleic acid fragments (siRNA) with LNPs, for the treatment of hereditary transthyretin-mediated amyloidosis of polyneuropathy[41]. For the mRNA vaccine against the new COVID-19 coronavirus disease, Moderna used an ionizable lipid SM-102[42], while Pfizer and BioNTech used an ionizable lipid called ALC-0315[43]. LNPs can not only effectively deliver mRNA to specific target cells to prevent mRNA from being degraded or cleared but

also help mRNA escape from cellular endosomes to the cytoplasm in a timely manner and be translated into corresponding proteins[44].

Given the rapid development of mRNA technology and the urgent application needs, the mRNA platform described in this study is composed of an uncapped mRNA structure without using N1mψTP in place of UTP. Our mRNA platform aims to improve product manufacturing efficiency, reduce costs, improve efficacy and ensure quality. By further optimizing the mRNA process and technical route, it is expected that our platform can provide more effective, longer-lasting and more efficient diversified treatment options for infectious diseases, rare diseases, cancer, chronic diseases and other diseases.

Results

Amplification of IVT template and preparation of uncapped mRNA with high yield and purity. As shown in Fig. 1a, the element sequences of the mRNA structure include the T7 promoter (T7P), internal ribosome entry sites (IRES), gene of interest (GOI) and poly A. Among them, the poly A region contains 106 repeating adenosine triphosphate bases. Five GOIs used in this study (gD^{ED}, gD^{FR}, $S^{\delta T}$, Fluc or eGFP) were each inserted between the IRES and poly A sequences of pT7AMP by homologous recombination. All constructed plasmids were verified by sequencing.

The IVT templates were obtained by PCR amplification using the above five plasmids as templates and primer pairs (T7-PF vs. pA-R). The electrophoresis results showed that the five IVT template fragments were all single bands with strong brightness, which was consistent with the expected fragment sizes (1834 bp, 2075 bp, 1670 bp, 2528 bp, and 4657 bp for the IVT templates for gD^{ED}, gD^{FR}, eGFP, Fluc, and $S^{\delta T}$ structures, respectively). The average concentration of IVT templates was 240±100 ng/μL, as determined by UV spectrophotometry or the Qubit method (Fig. 1b). Repeated experiments showed that PCR amplification could rapidly obtain IVT templates with relatively high concentration and purity.

IVT was performed with a PCR-amplified IVT template under DOE-optimized conditions. The mRNA purity was assayed by electrophoresis, and the concentration was determined by electrophoresis and the Qubit assay, and both of these measurements were monitored

posttranscriptionally. The concentrations of mRNA synthesized by 7 repeated IVT experiments were all within 4.3 ± 0.5 mg/mL, indicating that the mRNA yield synthesized by IVT optimized by DOE was high and robust (Fig. 1c). The mRNA synthesized by IVT was purified by a CIMmultus™ Oligo dT 18 chromatographic column, and a small amount of the purified mRNA was tested for its purity and concentration by HPLC. The SEC-HPLC test results showed that the number and area of cluttered peaks in the purified mRNA samples were reduced, indicating that the mRNA single peak area accounted for 99% of the total peak area (Fig. 1d).

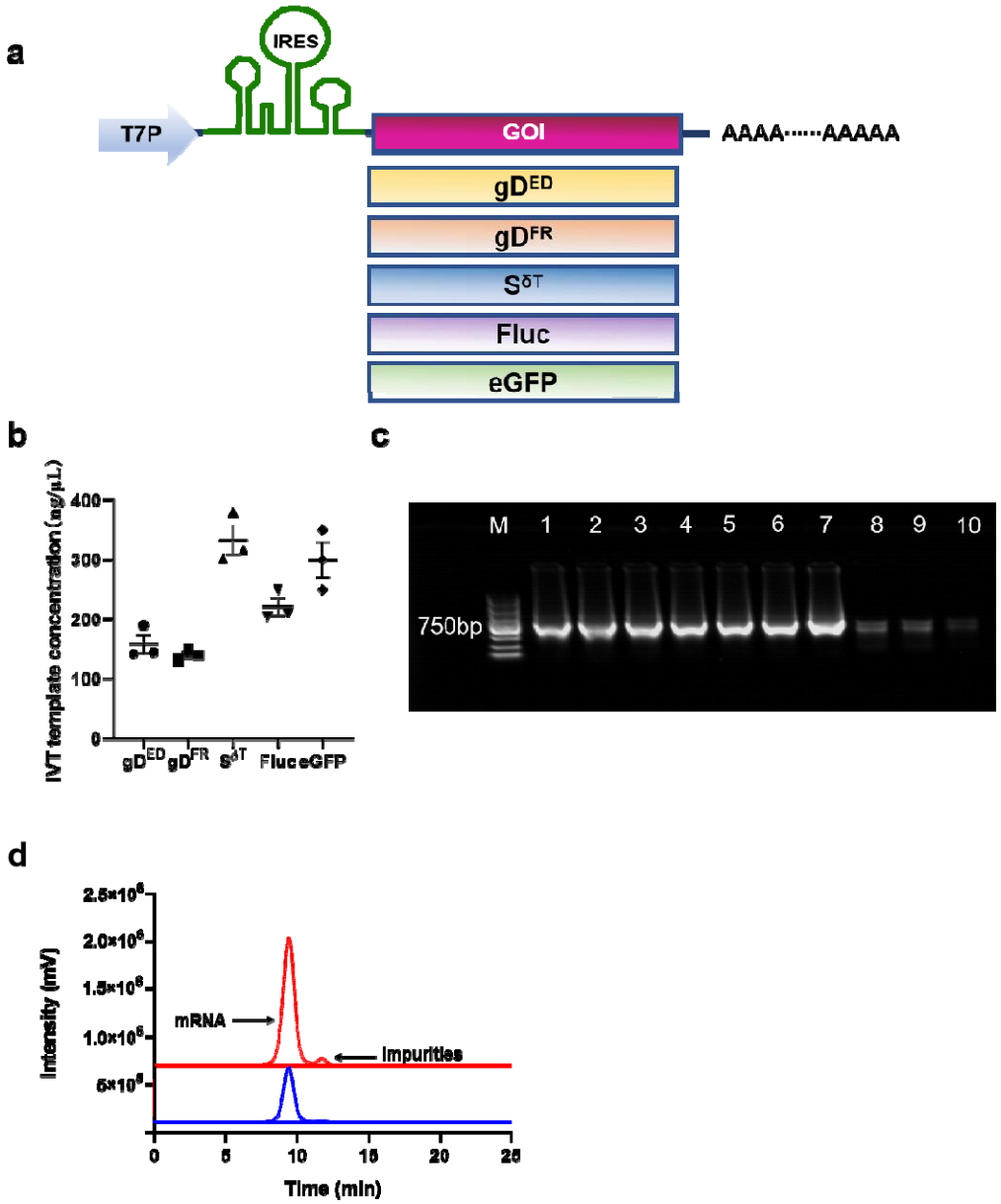

Fig. 1 | Amplification of the IVT template and preparation of uncapped mRNA with high yield and purity. a, Schematic diagram of mRNA structures. T7P and pA denote the T7 promoter sequence and polyadenosine sequence, respectively. **b,** Scatter plot of IVT template concentrations obtained by PCR amplification from 5 plasmid templates. Data are presented as the mean ± SEM (n=3). **c,** Agarose gel (1%) electropherogram of IVT-synthesized mRNA. Lanes 1-7 were the 7-repeat IVT products, the sample loading volume was 1 μL, and all IVT templates were Fluc mRNA; M was a 5000 bp DNA marker (Vazyme, China) with a loading volume of 5 μL; lanes 8, 9 and 10 were 900, 500, and 250 ng RNA references, respectively. **d,** SEC-HPLC analysis of mRNA samples obtained before and after purification with CIMmultus™ Oligo dT 18 (BIA Separations, Slovenia). Red and blue diagrams represent pre- and postpurified mRNA samples. The major peak area (representing purity) of the purified sample was greater than 99%.

Optimized encapsulation process can stably produce high-quality mRNA-LNPs. A total of six uncapped mRNA constructs, including gD^{ED}-mRNA, gD^{FR}-mRNA, S protein mRNA from the Delta strain ($S^{\delta T}$-mRNA), $S^{\delta T}$-$mRNA^{N1m\psi TP}$ (N1mψTP replaced UTP), Fluc-mRNA, and Fluc-$mRNA^{N1m\psi TP,}$ were encapsulated. The mRNA and lipid were mixed in a microfluidic mixer (Fig. 2a) to produce LNPs, which were analyzed by 1% agarose gel electrophoresis. After electrophoresis at 120 V for at least 30 minutes, all encapsulated mRNAs could not be removed and remained in the loading wells, and mRNA bands of expected sizes were not seen in the corresponding lanes (Fig. 2b). The results of mRNA concentration measurements showed that the encapsulation efficiency of the six mRNA molecules was greater than 90%. Table 1 shows the free mRNA content (C_f), total mRNA content (C_t) and encapsulation efficiency values after encapsulation of the six mRNA molecules. After removal of the nonaqueous solvent in the encapsulation system, each mRNA-LNP had a particle size (Z average) between 70 and 100 nm and a polymer dispensability index (PDI) less than 0.2 (Fig. 2c; Table 1).

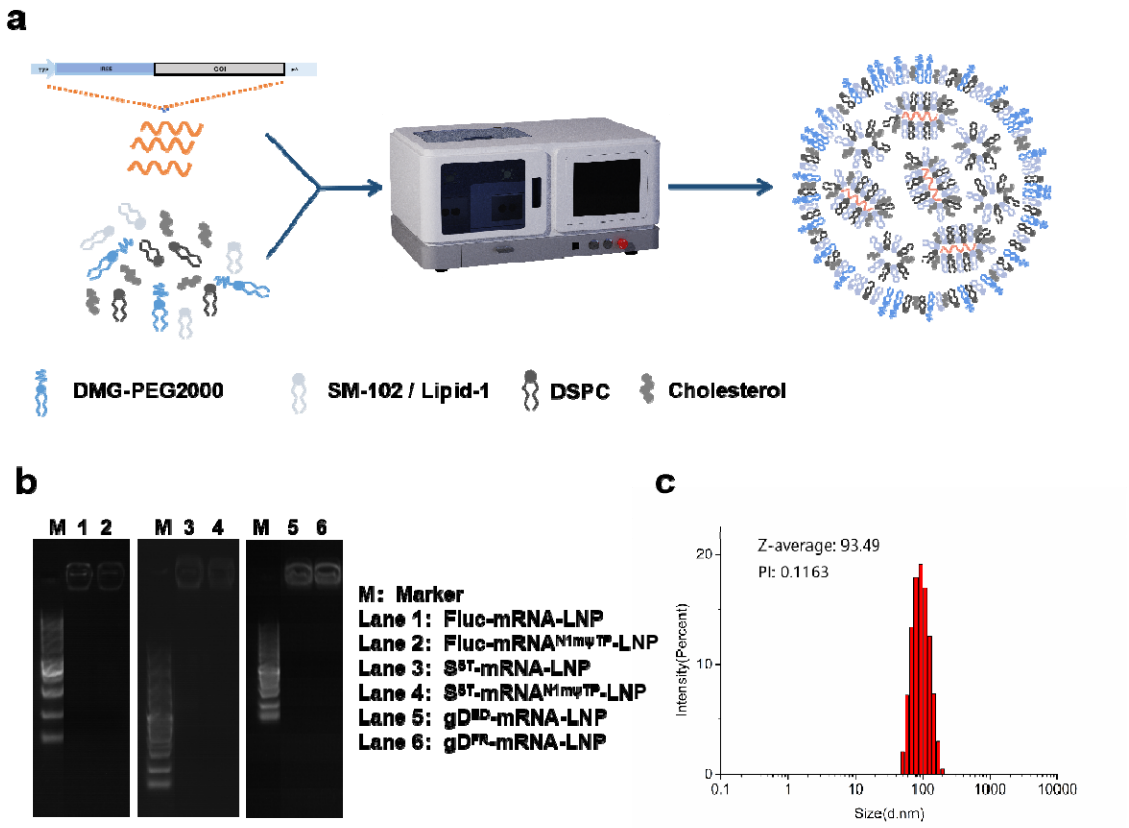

Fig. 2 | Encapsulation of mRNA. a, Process flow diagram. **b,** mRNA-LNP electrophoresis with parameters of 1% agarose gel, 120 V and TAE running buffer. M：Marker；Lane 1：Fluc-mRNA-LNP；Lane 2：Fluc$^{N1m\psi TP}$-mRNA-LNP；Lane 3：S$^{\delta T}$-mRNA-LNP；Lane 4：S$^{\delta T}$-mRNA$^{N1m\psi TP}$-LNP；Lane 5：gD^{ED}-mRNA-LNP；Lane 6：gD^{FR}-mRNA-LNP. **c,** Typical particle size of mRNA-LNP detected with a Mastersizer Laser Diffraction Particle Size Analyzer (Malvern).

Table 1. **Test data of key indicators of six mRNA-LNPs**

	C_f（ng/μL）	C_t（ng/μL）	EN（%）	Z-average（nm）	PDI
Fluc-mRNA-LNP	7.18	217	96.3	79.9	0.09
Fluc-mRNA$^{N1m\psi TP}$-LNP	5.44	258	97.9	74.5	0.12
S$^{\delta T}$-mRNA-LNP	5.54	290	98.1	80.9	0.07
S$^{\delta T}$-mRNA$^{N1m\psi TP}$-LNP	5.40	300	98.2	84.1	0.06
gD^{ED}-mRNA-LNP	11.0	320	96.5	85.6	0.08

gD^{FR}-mRNA-LNP	12.0	265	95.4	86.7	0.07

***In vitro* and *in vivo* expression of mRNA-LNP products containing indicator genes.** Our uncapped eGFP-mRNA-LNP can transfect a variety of cells, and the transfection method is simple and robust. Taking BHK cells as an example, after 4 hours of transfection with eGFP-mRNA-LNP (without removing eGFP-mRNA-LNP and changing the medium), eGFP green fluorescent protein was expressed in the cells, the cell morphology was normal, and the boundary was clear (Fig. 3a). The results showed that the uncapped eGFP-mRNA encapsulated by LNPs can quickly enter the cytoplasm through endocytosis and efficiently translate the target protein, and eGFP-mRNA-LNP did not show obvious cytotoxicity. The uncapped eGFP-mRNA-LNP can also be transfected into cells such as HEK 293T. The eGFP-mRNA-LNP products encapsulated with either SM102 or self-developed cationic lipids (Lipid-1) could easily and efficiently transfect cells to produce eGFP (Fig. 3b).

In vivo transfection of uncapped Fluc-mRNA-LNP (encapsulated with Lipid-1 and SM102) produced durable and high-yield expression. The mice were administered Fluc intramuscularly (n=5 for Lipid-1; n=3 for SM102), and the fluorescence intensity excited by Fluc in the mice was observed at different time points (Fig. 3c and 3h). The fluorescence intensity near the injection site first increased and then decreased with time, reaching a peak at 4~6 hours, and could continue *in vivo* for at least 72 hours for Lipid-1 and 94 hours for SM102 (Fig. 3e and 3g). These results indicated that the encapsulated Fluc-mRNA uncapped structure can be expressed efficiently *in vivo* in mice. Interestingly, the luciferase-fluorescence intensities and durability kinetics of our uncapped mRNA structure and the capped Moderna N1mψTP-mRNA structure at different time points were basically comparable (Fig. 3i and j).

In our uncapped mRNA structure, Fluc-mRNA-LNP outperformed Fluc-mRNA$^{N1m\psi TP}$-LNP in the *in vivo* transfection. Fluc-mRNA-LNP and Fluc-mRNA$^{N1m\psi TP}$-LNP were prepared using uncapped mRNAs. Four hours after intramuscular injection of mice, the total fluorescence intensity (p/s) of the Fluc-mRNA$^{N1m\psi TP}$-LNP group was $8.04\times10^{5}\pm1.43\times10^{6}$ (mean ± SEM, n=8), while the mean fluorescence intensity of the Fluc-mRNA-LNP group was $2.29\times10^{8}\pm1.04\times10^{8}$ (mean ± SEM, n = 4) (Fig. 3d and 3f). This result showed that our

uncapped mRNA-LNP did not necessarily need to use N1mψTP to achieve a higher expression level of the target protein *in vivo*.

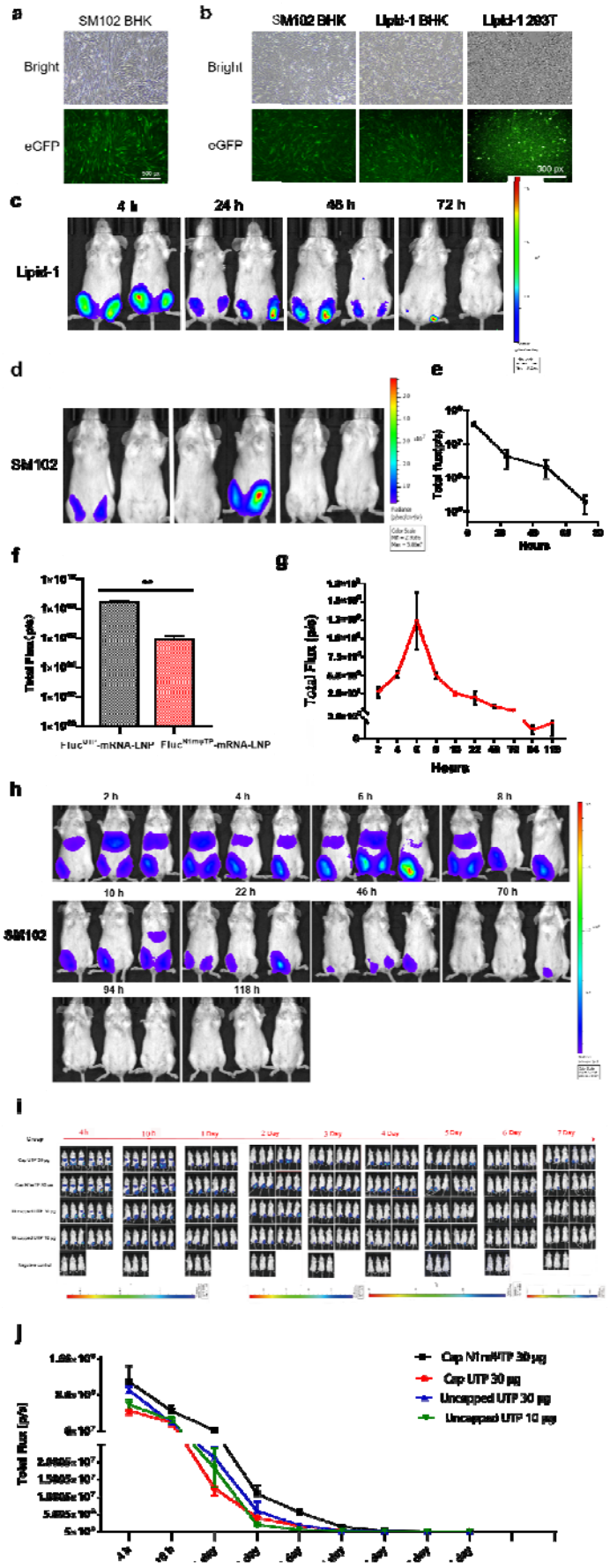
a
SM102 BHK
Bright
eGFP
b
SM102 BHK
Lipid-1 BHK
Lipid-1 293T
Bright
eGFP
c
4 h
24 h
48 h
72 h
Lipid-1
d
SM102
e
Hours
f
g
Total Flux (p/s)
Hours
h
2 h
4 h
6 h
8 h
10 h
22 h
46 h
70 h
94 h
118 h
SM102
i
j
Cap N1mΨUTP 30 μg
Cap UTP 30 μg
Uncapped UTP 30 μg
Uncapped UTP 10 μg

Fig. 3 | Uncapped mRNA-LNP transfection *in vitro* and *in vivo*. a, Bright-field and dark-field photos of BHK cells transfected with eGFP-mRNA-LNP for 4 hours. **b,** Bright-field and dark-field photos of BHK and HEK 293T cells transfected with eGFP-mRNA-LNP for 4 hours. **c,** The image of fluorescence intensity and **e,** the fluorescence quantitative histogram at various time points post transfection of Lipid-1-encapsulated Fluc-mRNA-LNP (30 μg/leg) into mouse muscle. **d,** Fluorescence intensity and **f,** fluorescence quantitative histogram 4 hours post-transfection of Fluc-mRNA-LNP and Fluc-mRNA$^{N1m\psi TP}$-LNP into mouse muscle. Two experiments were performed. As shown from left to right, animals 1 and 4 were injected with Fluc-mRNA-LNP at a dose of 20 μg/animal, while animals 2, 3, 5, and 6 were injected with Fluc-mRNA$^{N1m\psi TP}$-LNP at a dose of 20 μg/animal. **h,** The image of fluorescence intensity and **g,** the fluorescence quantitative histogram at various time points post-transfection of SM102 encapsulated Fluc-mRNA-LNP (20 μg/leg) into mouse muscle. **i,** Fluorescence intensity and **j,** fluorescence quantitative line chart at various time points.

Animals immunized with S$^{\delta T}$-mRNA-LNP but not S$^{\delta T}$-mRNA$^{N1m\psi TP}$-LNP produced high-titer binding and potent neutralizing antibodies. Day 0 was defined as the day of the first immunization in experiment 1, and mice were immunized on days 0 and 14 (Fig. 4a). The experiment was divided into three groups: the UTP group (30 μg/100 μL/animal, n = 3); the N1mψTP group (30 μg/100 μL/animal, n = 3); and the naïve group (without immunization, n = 3). On the 28th day, blood was collected to separate the serum and detect the serum IgG antibody titer. The results showed that the average titer of the UTP group reached 26666, whereas the titers for the N1mψTP group and the naïve group were under the detection limit (Fig. 4b). Statistical analysis showed that the titer of the UTP group was significantly different from that of the naïve group and the N1mψTPU group (P = 0.0048; *t*-test).

In experiment 2, the day for the first dose was designated as day 0, and Syrian hamsters were immunized with an intramuscular injection of S$^{\delta T}$-mRNA-LNP on days 0 and 21 (Fig. 4c). The experiment contained four groups: the 25 μg UTP group (25 μg/100 μL/animal, n = 3)); the 50 μg UTP group (50 μg/100 μL/animal, n = 3); the 100 μg UTP group (100 μg/100

μL/animal, n = 3); and the naïve group (without immunization, n = 3). On the 35th day, blood samples were collected to separate sera and detect serum binding (IgG) and neutralizing antibody titers. As shown in Fig. 4d, the average titers of IgG antibodies in the three experimental groups (25 μg, 50 μg, and 100 μg) were 3.47 ± 1.62E6, 2.35 ± 1.40E7 and 1.92 ± 0.64E7, respectively. It was noted that the antibody titers in experiment 2 were significantly higher than those in experiment 1, possibly due to differences in animal species, immunization doses and dose regimens. It was demonstrated that both SM102-encapsulated and Lipid-VI-encapsulated $S^{\delta T}$-mRNA-LNP produced high-titer IgG antibodies when used to immunize Syrian hamsters (Table. 2). The antibodies raised in Syrian hamsters with $S^{\delta T}$-mRNA-LNP can effectively neutralize both Delta and Omicron strains of SARS-CoV-2. The $S^{\delta T}$-mRNA-LNP doses and neutralization titers against Delta and Omicron strains are shown in Fig. 4e, which indicated that the $S^{\delta T}$-mRNA-LNP dose as low as 25 μg was able to induce potent neutralization antibodies to both Delta and Omicron strains after two immunizations.

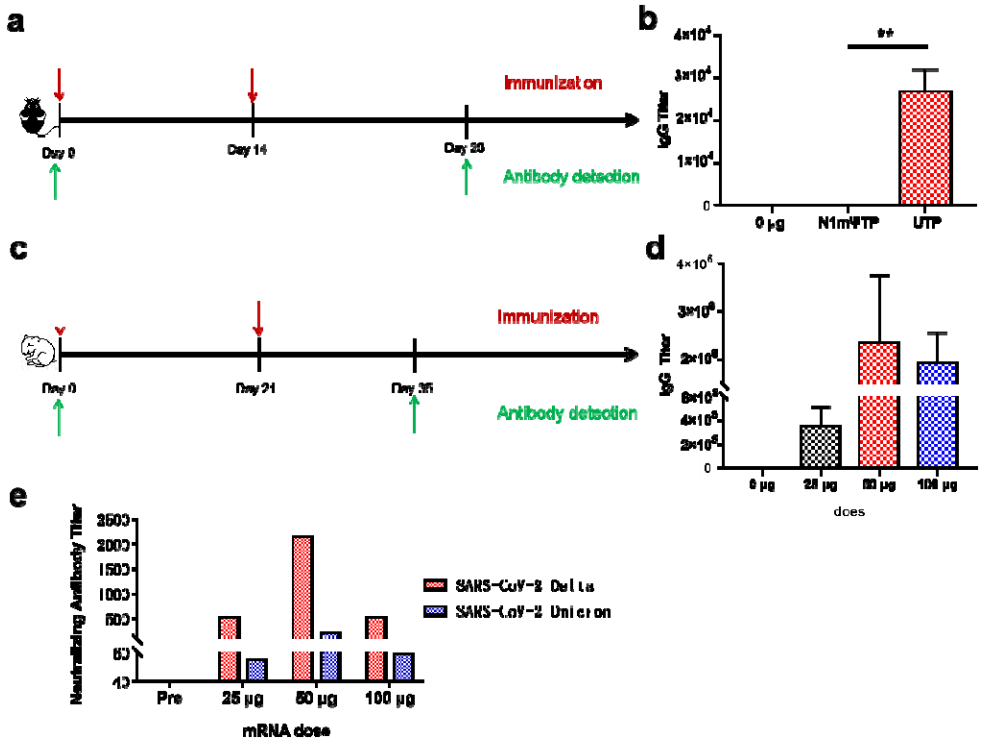

Fig. 4 | IgG and neutralization antibody detection after immunization with $S^{\delta T}$-mRNA-LNP and $S^{\delta T}$-mRNA$^{N1m\psi TP}$-LNP. a, Schematic diagram of immunization and serum sample collection in C57BL/6 mice. **b,** The SARS-CoV-2-specific IgG antibody titers of the 3 groups (0 μg, N1mψTP and UTP) were determined by ELISA. Significance was calculated using Student's *t*-test (**$p < 0.01$). **c,** Schematic diagram of immunization and sample collection in Syrian hamsters. **d,** The SARS-CoV-2-specific IgG antibody titers of the 4 groups (0, 25 μg, 50 μg, and 100 μg) on day 35 were determined by ELISA. **e,** Neutralization antibodies detected for SARS-CoV-2 Delta and Omicron strains in four groups (0 μg, 25 μg, 50 μg, and 100 μg; n = 1 for each group).

Table 2. Comparison of the immunogenicity of $S^{\delta T}$-mRNA-LNP encapsulated with Lipid-VI and SM102

LNP IgG Titer Dosage	50 μg	100 μg	200 μg
SM102	0.4×10^6	6.4×10^6	6.4×10^6
Lipid-VI	0.8×10^6	3.2×10^6	6.4×10^6

Animals immunized with gD^{ED}-mRNA-LNP and gD^{FR}-mRNA-LNP produced potent neutralizing antibodies. In the mouse experiment, the first immunization was designated as day 0. On days 0, 14 and 49, mice in the experimental groups were injected intramuscularly with gD^{ED}-mRNA-LNP (30 μg/100 μL/mouse, n = 5) or gD^{FR}-mRNA-LNP (30 μg/100 μL/mouse, n = 5) (Fig. 5a). On days 0, 28, and 56, blood samples were collected to separate sera for the detection of neutralizing antibodies. One microliter each of serum and oHSV2-eGFP virus containing 6250 $CCID_{50}$ were mixed well and incubated for 1 hour and then inoculated into the well containing a monolayer of Vero cells, and the neutralizing titer of the serum antibody was assessed by eGFP expression and plaque formation. As shown in Fig. 5b, all cells treated with the serum-virus mixture in the unimmunized group produced eGFP, and typical viral plaques resulting from virus replication could be seen. In contrast, eGFP and

viral plaques were not observed in cells treated with the serum-virus mixture (containing 6250 $CCID_{50}$ virus) in the gD^{ED}-mRNA-LNP and gD^{FR}-mRNA-LNP groups. The results indicated that the two HSV2 gD antigens expressed *in vivo* from our uncapped mRNA constructs could induce neutralizing antibodies in immunized C57BL/6 mice.

In another experiment, rabbits were used to assess the immunogenicity of gD^{ED}-mRNA-LNP in the induction of neutralizing antibodies. The initial immunization was designated as day 0. On days 0 and 14 of the experiment, 200 μL (20 μg) was injected intradermally into the hind neck of one rabbit, and 250 μL (25 μg) and 500 μL (50 μg) were injected into the muscles of the hind legs of the other two rabbits. At 0, 14, and 28 days, blood was collected from the middle ear artery to separate the serum to detect neutralizing antibodies (Fig. 5c). To assess the neutralizing potency of antibodies produced by gD^{ED}-mRNA-LNP after immunizing rabbits, live virus neutralization titrations were performed. Compared with the serum samples pre- and postimmunization, the serum samples postimmunization had clear neutralization activity of the virus (oHSV2-eGFP). In intradermally injected rabbits, 1 μL of serum completely neutralized 40960 $CCID_{50}$ viruses without eGFP expression or plaque formation (data not shown). Postimmunization serum from this rabbit had a neutralizing antibody titer (against 100 $CCID_{50}$ viruses) of 512 (Fig. 5d-b). However, the neutralization effect of the two rabbits injected intramuscularly was weaker than that of the intradermally injected rabbit. In the 25 μg intramuscularly injected rabbit, serum did not completely neutralize 100 $CCID_{50}$ viruses when diluted 16-fold (Fig. 5d-c). In the 50 μg intramuscularly injected rabbit, when the serum was diluted 64-fold, the 100 $CCID_{50}$ viruses could not be completely neutralized, and plaques appeared (Fig. 5d-e). The neutralization titers for the immunized dose and route difference are shown in Fig. 5e. To exclude the effect of complement on the experiment, we performed complement inactivation. The experimental results showed that the effect of the complement inactivation group was the same as that of the noninactivation group, and complement had no effect on the neutralization experiment (data not shown). It was concluded that rabbit serum samples following immunization (via intradermal or intramuscular injection) of gD^{ED}-mRNA-LNP could neutralize the oHSV2-eGFP virus.

a

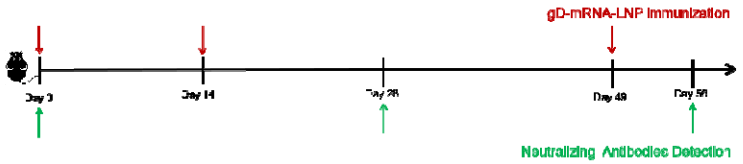
gD-mRNA-LNP Immunization
Day 3
Day 14
Day 28
Day 49
Day 56
Neutralizing Antibodies Detection

b

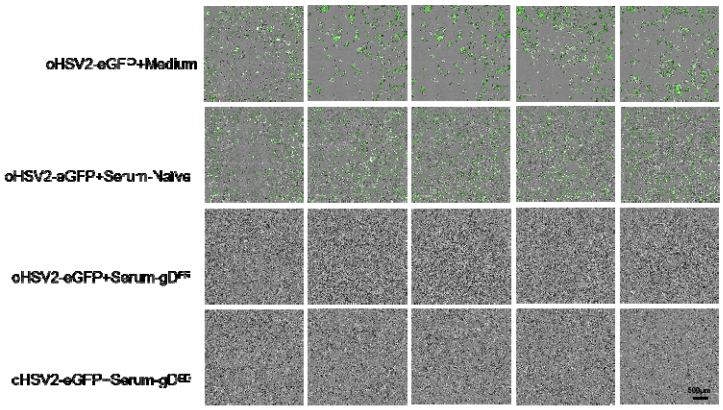
oHSV2-eGFP+Medium
oHSV2-eGFP+Serum-Naïve
oHSV2-eGFP+Serum-gD
cHSV2-eGFP+Serum-gD

c

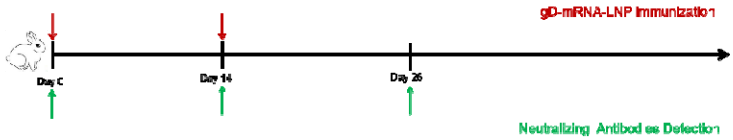
gD-mRNA-LNP Immunization
Day 0
Day 14
Day 28
Neutralizing Antibodies Detection

d

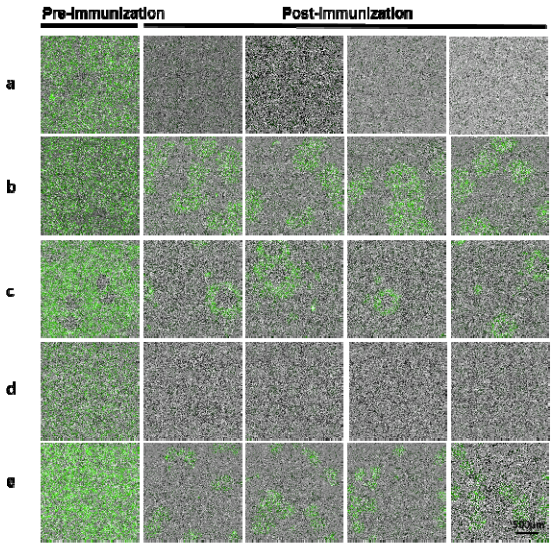
Pre-Immunization
Post-Immunization
a
b
c
d
e

e

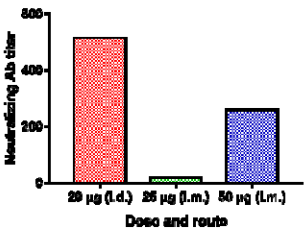
Neutralizing Ab titer
600
400
200
0
20 μg (i.d.)
25 μg (i.m.)
50 μg (i.m.)
Dose and route

Fig. 5 | Detection of the neutralizing antibodies produced by animals immunized with gD^{ED}-mRNA-LNP and gD^{FR}-mRNA-LNP using Vero cells and virus-infected plaques. a, Timeline of mouse immunization and blood collection. The red and green arrows represent the immunization time and the blood collection time, respectively. **b,** The postimmunization serum (at day 56) neutralization of oHSV2-eGFP. DME/F-12 containing neonatal bovine serum (termed Medium), preimmunization serum (termed Serum-Naïve), postimmunization serum from a mouse immunized with gD^{FR}-mRNA-LNP (termed Serum-gD^{FR}) and postimmunization serum from a mouse immunized with gD^{ED}-mRNA-LNP (termed Serum-gD^{ED}) were incubated with oHSV2-eGFP. **c,** Rabbit immunization regimen of gD^{ED}-mRNA-LNP. Three rabbits received two doses of gD^{ED}-mRNA-LNP immunization on days 0 and 14 (1 via intradermal injection, 2 via intramuscular). Blood was collected on days 0, 14 and 28 to separate the serum for the neutralization assay. **d,** The serum neutralization antibody titers (on day 28) were determined using Vero cells and plaques observed 72 hours post-virus infection for: (a) the 20 μg intradermal injection group with serum diluted 64 times; (b) the 20 μg intradermal injection group with serum diluted 512 times; (c) the 25 μg intramuscular injection group with serum diluted 16 times; (d) the 50 μg intramuscular injection group with serum diluted 32 times; and (e) the 50 μg intramuscular injection group with serum diluted 256 times. The constant amount of virus was 100 $CCID_{50}$/well, and the serum (collected at 28 days) was diluted for neutralizing antibody detection. **e,** The neutralizing antibody titers post gD^{ED}-mRNA-LNP immunizations at various doses and via different routes.

Cellular responses elicited in animals with uncapped gD-mRNA-LNP and S$^{\delta T}$-mRNA-LNP. The ELISpot assay showed that animals immunized with gD^{ED}-mRNA-LNP/gD^{FR}-mRNA- LNP or S$^{\delta T}$-mRNA-LNP produced specific T cells against the specific antigens. The primary immunization was recorded as day 0, and mice were immunized on designated days (Fig. 6a and 6d). In the experiment for gD^{ED}-mRNA-LNP/gD^{FR}-mRNA-LNP, three groups were designated: the gD^{ED}-mRNA-LNP group (30 μg/100 μL/unit, n=8); the gD^{FR}-mRNA-LNP group (30 μg/100 μL/unit, n = 8); and

the preimmunization (naïve) group (no immunization, n = 8). On the 21st day, the spleens of 4 mice in each group were taken for ELISpot detection (data not shown), the remaining 4 mice in each group were given a second booster immunization with the same dose, and the spleens of those mice were taken on the 28th day to detect specific T cells. After mixing 3×10^5 splenocytes with 10^6 $CCID_{50}$ of OH2 virus inactivated by UV (as stimuli) for 30 minutes and incubating for 48 hours, specific T cells were detected by the number of spots formed by IFN-γ cytokines secreted by splenocytes. As shown in Fig. 6b and Fig. 6c for the data with spleen taken on day 28, the average number of spots formed by IFN-γ cytokines in the two experimental groups (gD^{ED}-mRNA-LNP and gD^{FR}-mRNA-LNP) did have significant differences when compared with the average number of spots formed by IFN-γ cytokines in the naïve group. The results indicated that the two gD antigens translated *in vivo* by the uncapped mRNA structures could activate specific T cells in C57BL/6 mice. Similar results were obtained when mixing $S^{\delta T}$-mRNA-LNP-immunized splenocytes taken on day 32 (Fig. 6d) with SARS-CoV-2 S protein (as stimuli) followed by an ELISpot assay (Fig. 6e and 6f).

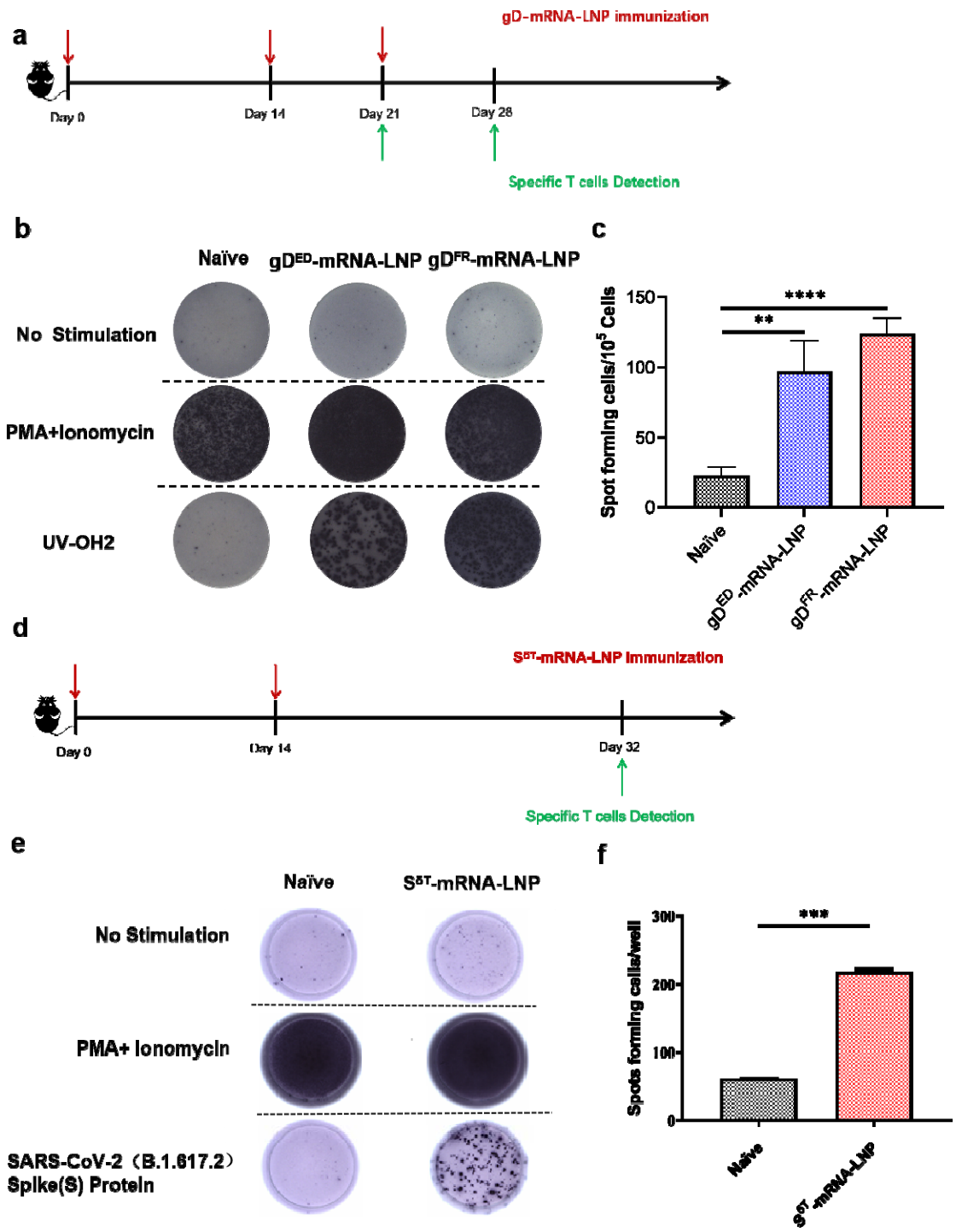

Fig. 6 | Animal T-cell immune responses after gD^{ED}-mRNA-LNP/gD^{FR}-mRNA-LNP or S$^{\delta T}$-mRNA-LNP immunization. a, and **d,** Timelines of the gD-mRNA-LNP or S$^{\delta T}$-mRNA-LNP immunization schedule and specific T-cell detection. The red and green arrows represent the immunization time and detection time, respectively. **b,** and **e,** The number of spots formed by IFN-γ cytokines secreted by splenocytes after immunization. **c,**

and **f,** Quantification of spot formation by IFN-γ cytokines secreted by splenocytes after immunization. Student's *t*-test (ns, not significant; *$p < 0.05$; **$p < 0.05$; ***$p < 0.001$; ****$p < 0.0001$).

Immunization with various mRNA-LNPs was able to induce high-titer specific antibodies. We also immunized rabbits with 5 different mRNA-LNPs encoding HSV2-UL19, HLA-E, NKG2A, hGM-CSF and HSV2-gL. All these mRNA-LNP treatments induced high levels of specific IgG at 10^5~10^6 titers. In addition, the antibodies were able to detect the antigens in their native forms: specific signals were obtained in immunofluorescence, flow cytometry, and western blot assays, in contrast to the pre-immune sera (Figure 7a-e). These data suggest that mRNA-LNP immunization can be sufficient to prime animals and induce high production of activated B cells suitable to produce specific antibodies.

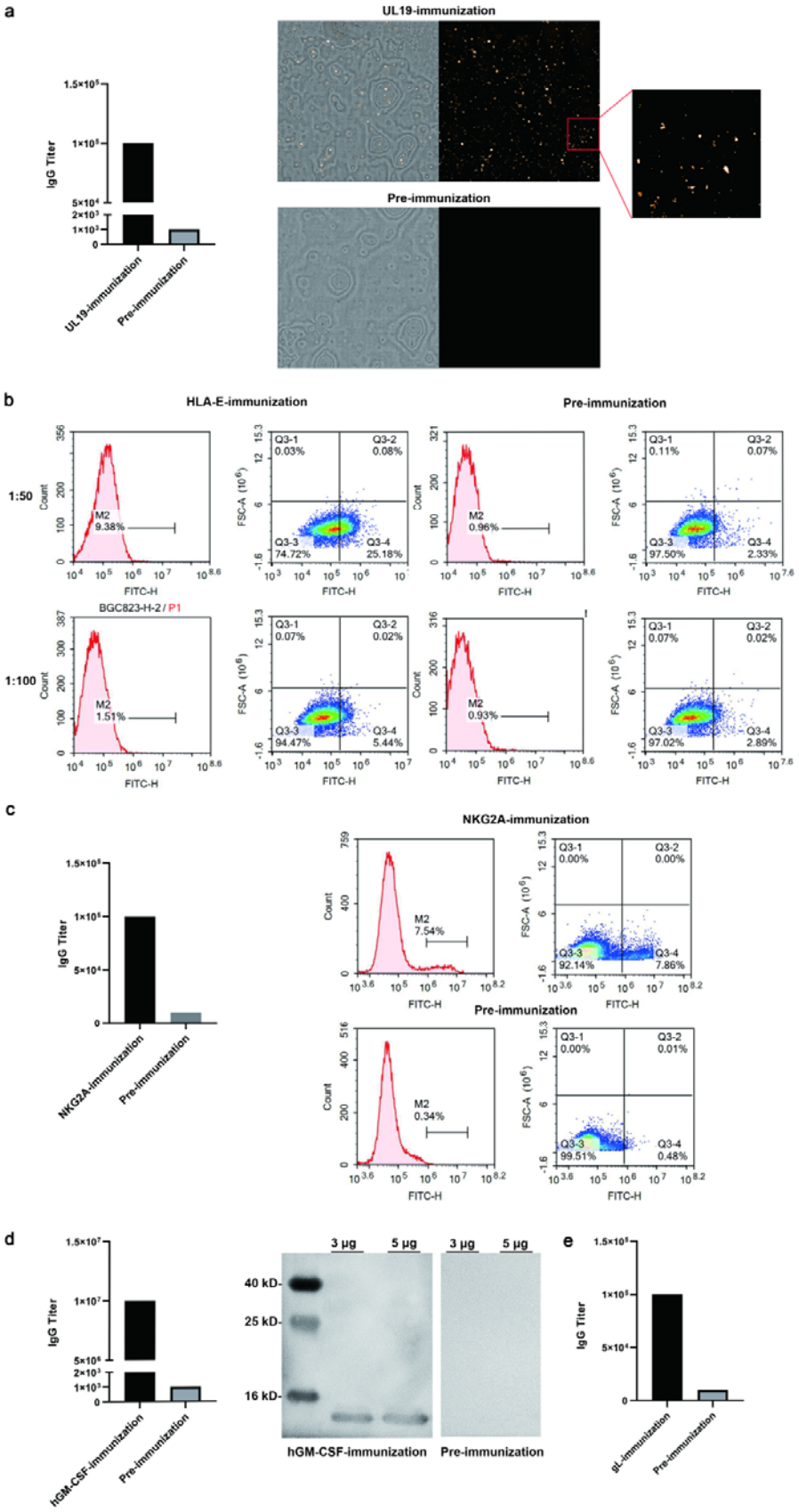
a
UL19-immunization
Pre-immunization
IgG Titer
UL19-immunization
Pre-immunization
b
HLA-E-immunization
Pre-immunization
1:50
1:100
BGC823-H-2 / P1
M2
9.38%
M2
0.96%
M2
1.51%
M2
0.93%
Q3-1
0.03%
Q3-2
0.08%
Q3-3
74.72%
Q3-4
25.18%
Q3-1
0.11%
Q3-2
0.07%
Q3-3
97.50%
Q3-4
2.33%
Q3-1
0.07%
Q3-2
0.02%
Q3-3
94.47%
Q3-4
5.44%
Q3-1
0.07%
Q3-2
0.02%
Q3-3
97.02%
Q3-4
2.89%
Count
FSC-A
FITC-H
c
NKG2A-immunization
Pre-immunization
IgG Titer
NKG2A-immunization
Pre-immunization
M2
7.54%
Q3-1
0.00%
Q3-2
0.00%
Q3-3
92.14%
Q3-4
7.86%
M2
0.34%
Q3-1
0.00%
Q3-2
0.01%
Q3-3
99.51%
Q3-4
0.48%
d
IgG Titer
hGM-CSF-immunization
Pre-immunization
3 μg
5 μg
3 μg
5 μg
40 kD
25 kD
16 kD
hGM-CSF-immunization
Pre-immunization
e
IgG Titer
gL-immunization
Pre-immunization

Fig. 7 | Analysis of the specificity of the rabbit antisera after mRNA-LNP injection. Rabbits were immunized 4 times with 50 μg of mRNA-LNPs by intradermal injection at 2 week intervals. Serum was collected 5 days after the final injection. a, HSV2-UL19-specific IgG levels were determined by endpoint dilution ELISA (left panel), and binding reactivity to HSV2 particles was measured by immunofluorescence (right panel). The data in the immunofluorescence assay were obtained at 1:1000 dilution. **b,** Serum from a rabbit injected with HLA-E mRNA-LNPs was tested for binding reactivity to BGC823 cells by flow cytometry assay. BGC823 cells were stimulated with HSV2 (MOI=1) to increase HLA-E expression. The antiserum of a rabbit immunized with HLA-E mRNA-LNPs displayed a positive reaction with BGC823 cells, while no signals were detected with the pre-immune serum. **c,** NK92 cells was stimulated with IL-2 to increase NKG2A expression and incubated with serially diluted sera. The antiserum of a rabbit immunized with NKG2A mRNA-LNPs showed a rightward shift (right panel) compared to its pre-immune control. **d,** IgG levels against hGM-CSF were determined by ELISA (left panel) and western blot assay (right panel). The data in the immunofluorescence assay were obtained at 1:1000 dilution. **e,** IgG levels against HSV2 gL were determined by ELISA.

Discussion

Our mRNA platform has 4 notable features: Rapid, Amplified, Capless, and Economical (RACE; registered as the BH-RACE platform). Using IRES to replace the cap structure, using UTP but not N1MψTP to synthesize mRNA, and using self-developed encapsulation instruments and LNP delivery systems can greatly reduce the cost of raw materials, simplify the production process, and shorten the production time. At the same time, it has been shown that both the new coronavirus S protein mRNA vaccine and HSV2 gD protein mRNA vaccines can activate both humoral and cellular immunity in animals. Particularly exciting is that potent neutralizing antibodies against Delta and Omicron real viruses were induced with the new coronavirus S protein mRNA vaccine from the BH-RACE platform.

The application prospects of mRNA technology are very broad, and this technology can be used for the development of mRNA vaccines, protein replacement drugs and rapid antibody

preparations. mRNA vaccines include prophylactic and therapeutic mRNA vaccines[45]. Prophylactic mRNA vaccines can express specific protein antigens when delivered into the body, thereby activating the immune response to prevent infectious diseases. Such vaccines are being widely developed for viruses including the new coronavirus (mRNA-1273, BNT162b2), the herpes simplex virus (Moderna, mRNA-1608; Binhui Bio, HSV2 gD mRNA vaccine)[46], the influenza virus (mRNA-1010, BNT161, CVSQIV), the Zika virus (mRNA-1893), HIV (mRNA-1644), and the rabies virus (CureVac, CV7202, https://www.curevac.com/en/pipeline/). Therapeutic mRNA vaccines are mainly antitumor vaccines, including dendritic cell (DC)-based mRNA vaccines[47] and directly administered mRNA vaccines[48]. For DC vaccines, mRNA is transfected into DCs *in vitro* and translated into antigens, which are processed and presented by DCs. Antigen-presenting DCs are then injected into the body to stimulate an antitumor immune response. For directly administered mRNA vaccines, the mRNA encoding the relevant antigen with or without a cytokine as an adjuvant (e.g., granulocyte-macrophage colony-stimulating factor, GM-CSF) is injected into the body, thereby activating the immune response and inhibiting the growth of tumors[49]. At present, a number of mRNA tumor vaccines are under development, mainly including Moderna pipelines (mRNA-4157, personalized cancer vaccine; mRNA-5671, KRAS vaccine), BioNTech pipelines (BNT111, advanced melanoma; BNT-113, HPV16+ head and neck cancer; BNT-122, adjuvant colorectal cancer), CureVac pipelines (CV-8102, oncology candidate; undisclosed, tumor-associated antigens), and Binhui pipelines (heterologous mRNA tumor vaccines). For protein replacement drugs, mRNA is delivered into cells and translated into the corresponding protein to treat rare diseases caused by the deletion or mutation of this protein. These include Moderna's mRNA-3705 for the treatment of methylmalonic acidemia (MMA), mRNA-3927 for the treatment of propionic acidemia (PA)[50], and Sanofi's SAR339375 for the treatment of Alport syndrome (https://www.sanofi.com/en/science-and-innovation/). Regarding rapid antibody preparation, the mRNA-LNP antigen is designed to replace the traditional protein antigen, which facilitates the quick preparation of polyclonal and monoclonal antibodies. This fast antibody preparation technology has the advantages of many types of applicable antibodies, a short preparation period, high specificity and high purity. At

present, Binhui Bio has used the mRNA platform to prepare an HSV2 gD monoclonal antibody (data not shown), which will be used to assist the development of an mRNA vaccine against HSV2.

The mRNA 5' cap structure determines the "self" and "nonself" mRNA properties. Nonself mRNAs recognized by host cells can trigger strong host immune responses against nonself RNAs through toll-like receptors 3, 7-9[51]. Furthermore, the IRES sequence from Cytomegalo encephalitis virus used in our mRNA constructs could theoretically elicit a severe anti-RNA immune response leading to rapid RNA degradation and reduced protein expression over time, making it very unlikely to induce the antigen-specific immune response desired for the target protein. However, our results showed that (1) *in vivo* transfection of our LNP-encapsulated Fluc mRNA (one of our uncapped mRNA constructs) resulted in high levels of expression with signal intensities as high as $E^{8\text{-}9}$ total flux p/s, similar to the expression levels of *in vivo* transfection of LNP-encapsulated capped Fluc mRNA[52]; (2) immunization of mice, hamsters and rabbits with our uncapped mRNA constructs induced high titers of IgG and neutralizing antibodies against the designed targeting protein antigens, and (3) our uncapped mRNA constructs are able to induce target protein specific cellular immune responses.

mRNA vaccines activate humoral and cellular immunity in animals. The mice (C57BL/6) and rabbits (Japanese White Rabbit) were both immunized with our uncapped mRNA constructs encoding HSV2 truncated gD proteins. ELISpot (IFN-γ) assays (not performed on the rabbits) showed that the cellular immunity of the mice was activated, and the neutralization tests showed that sera from both animal species contained neutralizing antibodies. It was noted that immunization of rabbits via two routes (intramuscular and intradermal) resulted in the production of antibodies with different neutralizing titers, which is consistent with a previous report[53]. In addition, mice (C57BL/6) and Syrian hamsters were immunized with uncapped mRNA encoding the new coronavirus spike protein trimer of the Delta strain ($S^{\delta T}$-mRNA-LNP). The ELISpot (IFN-γ) assay (not performed on the hamsters) showed that the cellular immunity of the mice was activated. ELISA could also detect serum IgG antibodies from both animal species. However, the serum IgG antibody titers of both animal species were significantly different. It has been reported that animals of different

species immunized with the same mRNA vaccine could produce IgG antibodies with different titers[54]. In our study, using $S^{\delta T}$-mRNA-LNP to immunize Syrian hamsters, the doses of 50 μg and 100 μg appeared to be more potent in the generation of high titer antibodies than the dose of 25 μg, indicating that the doses of mRNA vaccines might be related to the immune effects.

Our mRNA technology platform described here is notable for its uncapped mRNA construct and the omission of any nucleotide modification for the mRNA sequence. These characteristics form a clear contrast to those of the demonstrated and successful mRNA technology platforms developed by others, which are characterized by 5' capped mRNA structures (Moderna, BioNTech and CureVac) and complete pseudouridine modification[25, 55] (Moderna and BioNTech) on the mRNA sequences. Using neither the 5' cap structure nor nucleotide modification undoubtedly not only reduces the cost of the raw materials but also simplifies the manufacturing process, representing a step forward in this field.

Although there is still a lack of sufficient studies about whether the IRES-driven translation of mRNA is affected by nucleoside modification in the primary RNA sequences, our data presented here suggest that nucleoside modification reduces antigen expression and the resulting antigenicity. We obtained a competitive high titer of total IgGs from our special mRNA platform. Another emerging and unanswered question is whether the total IgGs induced by the IRES-facilitated antigen expression from the unmodified mRNA are correlated with TLR recognition. Exogenous RNAs without nucleoside modification are treated as pathogens in mammalian cells and stimulate innate immunity via their interaction with TLRs, therefore leading to a short lifespan[25] and theoretical insufficient target antigen expression levels. Our mRNAs containing the 5' IRES structure without nucleoside modification successfully avoided elimination by the innate immune system. The mechanism underlying this phenomenon is interesting and needs to be explored further.

However, we should note that there still exist a few issues to be addressed. First, regarding the nucleoside modification in the mRNA sequences, we only compared the use of pseudouridine to replace the natural uridine but have not yet addressed other types of nucleoside modifications, such as m5C, m6A, N7-methylguanosine (m7G), or a combination of m5C and m7G. Last but not least, the uncapped mRNA constructs used in this work for the

immunogenicity assays were mostly delivered using an LNP formulation developed by Moderna. Of note, a proprietary mRNA delivery system that might be more suitable for our proprietary mRNA structure is awaiting development.

Methods

Plasmid construction. The construction of the plasmid template for *in vitro* transcription (IVT) is as follows: all the constructed plasmids are derived from pT7AMP (constructed in our laboratory, to be published soon). The coding sequences for two truncated D-type envelope glycoproteins from herpes simplex virus type 2 (HSV2 gD^{ED} with amino acid sequence 1-316 and HSV2 gD^{FR} with amino acid sequence 1-400), the coding sequence for SARS-CoV-2 spike protein trimer from Delta strain, termed $S^{\delta T}$ with amino acid sequence 1-1274aa (including proline mutations at positions 982 and 983[56], RRAR to GGSG mutations at 678-681aa for S1/S2 cleavage site and a trimerization domain at positions 1203-1274aa), the coding sequence for firefly luciferase (Fluc), the coding sequence for enhanced green fluorescent protein (eGFP) and the sequence for poly A (106 bp) were synthesized by GenScript (Nanjing, China). The above synthesized fragments were cloned into the *BglII* site of the ampicillin-resistant pT7AMP vector by homologous recombination to obtain plasmids pT7AMP-gD^{ED}, pT7AMP-gD^{FR}, pT7AMP-$S^{\delta T}$, pT7AMP-Fluc, and pT7AMP-eGFP. All the constructed plasmids were verified by sequencing. The plasmids were transformed into *Escherichia coli* followed by picking a single colony to be cultured in LB medium containing ampicillin (100 μg/mL) at 37 °C with orbital shaking at 200 rpm for 16-24 hours. After that, the plasmids were extracted with a kit (Vazyme Biotech Co., Ltd, DC201-01) and stored in aliquots at -20 °C.

mRNA IVT template preparation. The plasmids described above were used as templates and primer pairs (T7P-F: agggaataagggcgacacggaaatgttgaatactcat and pA-R: ggattgggaagacaatagcaggcatgctgggg, synthesized by Wuhan Qingke Biotechnology Co., Ltd.) were used for PCR amplification with the high-fidelity enzyme 2×Phanta® Flash Master Mix (Vazyme Biotech Co., Ltd., P510-03) to obtain mRNA transcription templates. A small

amount of PCR product was taken for concentration detection using a Qubit 4.0 Fluorometer (Thermo) with a Qubit™ dsDNA HS Assay Kit (Q32854). The PCR product quality was also assayed by electrophoresis on a 1% agarose gel at 120 V for 30 minutes followed by visualization with a gel imaging system.

***In vitro* transcription (IVT).** IVT was optimized by DOE (Design Of Experiment). The optimized reaction system (200 μL) contained: ATP 5 mM (Roche, Mannheim), CTP 5 mM (Roche, Mannheim), GTP 5 mM (Roche, Mannheim), UTP 5 mM (Roche, Mannheim), recombinant T7 RNA polymerase 1200U (Roche, Mannheim), DNA template (20~35 ng/μL), inorganic pyrophosphatase 3U (Roche, Mannheim), RNase inhibitor 40U (Roche, Mannheim), 10×Transcription Buffer 20 μl (recipe: 400 mM Tris-HCl with pH=7.9, 240 mM $MgCl_2$, 20 mM spermidine, 100 mM DTT for dithiothreitol and DEPC for diethylpyrocarbonate water). To synthesize N1-methyl pseudouridine triphosphate (N1mψTP)-modified mRNA, UTP was replaced with N1mψTP (Wuhan Tangzhi Biotechnology Co., Ltd., Wuhan, China). After 3 hours at 37 °C, DNase I (Shanghai Jingan Protein Biotechnology Co., Ltd.) was added to degrade the DNA in the reaction system. Finally, the IVT mRNA product was aliquoted and stored at -80 °C.

IVT mRNA purification. mRNA was purified using an AKTA Avant chromatography system (GE, Sweden) and a CIMmultus™ Oligo dT 18 chromatography column (BIA Separations, Slovenia). The mRNA sample was mixed with OA (Oligo dT Adjust) buffer (recipe: 50 mM phosphate buffer, 2 mM EDTA, 1 M NaCl) at a ratio of 4:1 to adjust the ionic concentration of the sample solution. The mixed sample was injected into the AKTA sample loop, and the mRNA was adsorbed by the column. After injection, the column was washed with OW (Oligo dT Wash) buffer (recipe: 50 mM phosphate buffer, 2 mM EDTA). The mRNA was eluted from the column using water for injection (in-house) to obtain the purified mRNA stock solution. Finally, the concentration and purity of the mRNA stock solution were detected by SEC-HPLC (SHIMADZU, Japan) using an analytical TSK G6000 PWXL column (TOSOH, Japan). The mobile phase was 0.02 M phosphate buffer (homemade) at a flow rate of 1

mL/minute.

Preparation of lipid nanoparticles (LNPs). The LNP formulation was optimized on the basis of the literature[50]**.** Four components, including SM 102 (Xiamen Sinopeg), or our self-designed ionizable amino lipids (Lipid-1 and Lipid-VI), DSPC (1,2-distearoyl-sn-glycero-3-phosphocholine, purchased from AVT), cholesterol (AVT) and PEG (polyethylene glycol, purchased from AVT), were dissolved in ethanol at a molar ratio of 50:10:38:2. The obtained lipid mixture was then mixed with 25 mM sodium acetate (pH=5.0) buffer at 1:4 (ethanol:water) in a microfluidic mixer (Precision Nanosystems, Canada or NanoPro System, self-developed). The ionizable N:P ratio in the formulation was 4:1. The encapsulated mRNA-LNPs were concentrated by changing the buffer (20 mM Tris solution containing 8% sucrose, pH=7.2~7.4) using a centrifugal filter (Amicon Ultra, Millipore, 30 kDa) or a Tangential Flow Filtration (TFF) membrane (Sartorius, 30 kDa). The mRNA-LNP concentrates were sterilized through a 0.22-micron filter and stored in aliquots at 4 °C or -80 °C.

Detection of mRNA encapsulation efficiency. mRNA concentrations were measured on a Qubit 4.0 Fluorometer (Thermo) using the Qubit® RNA BR Assay kit (Thermo). According to the instructions, the unencapsulated mRNA content (C_f) and the mRNA content (C_t) of the same sample after adding 0.1% (v/v) Triton X-100 (Sigma) were measured to calculate the mRNA encapsulation efficiency. The encapsulation rate was calculated as $(1-C_f/C_t)\times100\%$.

***In vitro* transfection.** BHK (Baby Hamster Kidney) and HEK 293T (human embryonic kidney 293T) cells were purchased from ATCC; fetal bovine serum (FBS) was purchased from Zhejiang Tianhang Biotechnology Ltd. (110-11-86-11); high-glucose DMEM was purchased from Procell (PM150210); 6-well plates were purchased from BIOFIL (TCP10006). BHK or HEK 293T cells were seeded in 6-well plates at 2×10^5 cells/well. After 24 hours, when the cell confluence reached 60~70%, the medium in the well was replaced with 2 mL of fresh high-glucose DMEM containing 5% FBS. eGFP-mRNA-LNP (at 3~4 μg mRNA/well)

was slowly added along the wall of the well, and the plate was shaken evenly. The cells were cultured at 37 °C and 5% CO_2 for 4 hours, followed by microscopic observation of the cells transfected with eGFP-mRNA-LNP.

Animal experiments. All animal experiments were carried out in strict accordance with the requirements of the Hubei Provincial Committee for the Management and Use of Laboratory Animals. Six- to eight-week-old female C57BL/6 mice (Certificate number: No.42000600043578) and female BALB/c mice (Certificate number: No.42000600046737), 5-week-old female Syrian hamsters (Certificate number: No.42000400012878), and 5-week-old female Japanese white rabbits (Certificate number: No.42010000006599) were purchased from the Hubei Provincial Center for Disease Control and Prevention. Animals had free access to water and food in a controlled environment with a 12-hour light/dark cycle.

In vivo transfection of Fluc-mRNA-LNP: LNP-encapsulated Fluc-mRNA was injected intramuscularly in the thighs of mice. At designated time points, 100 μL of D-fluorescein potassium salt (Beyotime, 15 mg/mL) was intraperitoneally injected, and images were recorded using an IVIS imaging system (Perkin Elmer) approximately 10 minutes later.

Immunization of $S^{\delta T}$-mRNA-LNP: At two time points (mice at days 0 and 14; hamsters at days 0 and 21), LNP-encapsulated $S^{\delta T}$ mRNA was injected into the thigh muscle of mice or hamsters. Orbital blood and heart blood samples were collected from mice and hamsters, respectively, before and after immunization, and the serum samples were separated for the detection of IgG antibody titers and/or neutralizing antibody titers.

Immunization with HSV2 gD-mRNA-LNP: At three time points (days 0, 14, and 49), LNP-encapsulated gD-mRNA products were injected intramuscularly into the thighs of mice. Orbital blood samples were collected from mice before and after immunization, and serum samples were separated for neutralizing antibody detection.

At two time points (day 0 and day 14), different doses of LNP-encapsulated gD-mRNA preparations were injected into the rabbits at the posterior neck intradermally or at the hind leg intramuscularly, respectively. Before and after immunization, rabbit middle ear venous blood samples were collected, and serum samples were separated for neutralizing antibody

detection.

ELISA detection of antibodies. SARS-CoV-2 (B.1.617.2) spike (S) protein was purchased from Nanjing Vazyme Biotechnology Co., Ltd. (GC221-01); Tween-20 was purchased from Sinopharm Chemical Reagent Co., Ltd. (Cat. No. 30189328); bovine serum albumin (BSA) was purchased from BioFroxx (Cat. No. 4240GR025); 96-well microtiter plate was purchased from Thermo (Cat. No. 446469); sulfuric acid was purchased from Sinopharm Chemical Reagent Co., Ltd. (Cat. No. 10021628). The detection steps of SARS-CoV-2 S protein-trimer-specific IgG antibody are as follows: The microtiter plate was coated with SARS-CoV-2 (B.1.617.2) S protein at 100 ng/well and left overnight at 4 °C. The next day, the plate was washed with washing solution (PBST with 0.05% Tween-20) and blocked with PBST containing 1% BSA for 2 hours. Mouse serum samples were serially diluted 2-fold starting from 1:1000. The hamster serum samples were diluted to $1:2\times10^4$ and then serially diluted 2 times. The diluted serum samples were sequentially added to the plate followed by incubation at 37 °C for 60 minutes. After washing the plate 3 times with washing solution, the corresponding diluted solution of horseradish peroxidase (HRP)-conjugated antibody (goat anti-mouse IgG 1:2000, Proteintech; rabbit anti-hamster IgG 1:5000, Jackson ImmunoResearch, 307-035-003) was added followed by incubation at 37 °C for 60 minutes. After fully washing the plate with washing solution, TMB solution (Solarbio, PR1200) was added, followed by incubation at 37 °C for 5 minutes. Next, the color production of each well was stopped with 2 M sulfuric acid. Finally, the absorbance (at a wavelength of 450 nm) of each well was read using a microplate reader (Thermo).

Detection of neutralization antibodies. Delta (YJ20210701-01) and Omicron (249099) variants of SARS-CoV-2 were provided by Hubei Provincial Center for Disease Control and Prevention. All SARS-CoV-2 live virus experiments were performed in the Biosafety Level 3 (BSL-3) facility at the Institute of Health Inspection and Testing, Hubei Provincial Center for Disease Control and Prevention.

Neutralization of serum antibodies was assessed by a constant virus amount. Serum

samples were serially diluted 2-fold starting from 1:8. Each of the diluted serum samples was thoroughly mixed with the oHSV2-eGFP (an HSV2 virus expressing eGFP made in our lab) virus or SARS-CoV-2 (Delta and Omicron strains) solution containing 100 $CCID_{50}$ (or $TCID_{50}$) to obtain a serum-virus mixture that was incubated at 37 °C for 1 hour in the presence of penicillin (100 U/mL) and streptomycin (0.1 mg/mL). Then, each serum-virus mixture was inoculated into the corresponding well of a 96-well microtiter plate cultured with a monolayer of Vero cells and incubated at 37 °C in 5% CO_2 for 48~96 hours. Fluorescence expression for gD neutralization antibody titer or cytopathic effect (CPE) for SARS-CoV-2 S protein neutralization antibody titer in the wells was observed using the High Content Analysis System (Perkin Elmer) or microscope, respectively. Antibody neutralization titers were assessed by the Reed-Muench method[57].

Alternatively, the neutralizing activity of serum antibodies was assessed by constant serum dilutions. The oHSV2-eGFP virus was serially diluted 2 times from 1:2 to obtain suspensions containing different amounts of virus (1500-100000 $CCID_{50}$). Each virus suspension was thoroughly mixed with serum to obtain a virus-serum mixture that was incubated at 37 °C for 1 hour in the presence of penicillin (100 U/mL) and streptomycin (0.1 mg/mL). Then, each virus-serum mixture was inoculated into the corresponding well of a 96-well microtiter plate cultured with a monolayer of Vero cells and incubated at 37 °C in 5% CO_2 for 48 hours. Fluorescence expression in wells (representing cytopathic effect, CPE) was detected using the High Content Analysis System. The neutralizing activity of serum antibodies was evaluated by CPE.

ELISpot tests on animals immunized with uncapped mRNA-LNP. At 2-3 time points (days 0, 14, and 21), LNP-encapsulated mRNA was injected intramuscularly into the thighs of mice. At a designated time point, the immunized mouse spleens were removed, and splenocytes were isolated for the detection of specific T cells.

A mouse IFN-γ ELISpotPLUS kit was purchased from Mabtech (Cat. No.: 3321-4APW-2); PMA+ionomycin was purchased from Shenzhen Dakewe Bioengineering Co., Ltd. (Cat. No. 2030421); SARS-CoV-2 (B.1.617.2) S Protein was purchased from Nanjing Vazyme

Biotech Co., Ltd. (Cat No GC221-01). OH2 (oHSV2-hGM-CSF[58] derived from the HSV2 HG52 strain) virus was prepared by our laboratory. The detection steps of gD-specific or $S^{\delta T}$-specific T cells were as follows: 3-5×10^5 splenocytes/well and 10^6 $CCID_{50}$/well OH2 virus inactivated by UV for 30 minutes (or 4 μg/well SARS-CoV-2 S Protein) were mixed and incubated at 37 °C. After 48 hours followed by 5 washes with PBS, probe antibody (R4-6A2 biotin, 1 μg/μL) was added and incubated at room temperature for 2 hours. After washing with PBS 5 times, alkaline phosphatase-labeled streptavidin (Streptavidin-ALP, 1:1000) was added and incubated for 1 hour at room temperature. After washing with PBS 5 times, alkaline phosphatase-labeled streptavidin (Streptavidin-ALP, 1:1000) was added and incubated for 1 hour at room temperature. After washing 5 times with PBS, chromogenic solution (BCIP/NBT-plus) was added and incubated at room temperature for 10 minutes. Color development was then stopped with deionized water. Once dried, the number of spots presented in the wells on the ELISpot plate was read and analyzed using an enzyme-linked spot analyzer (AID ELISpot Reader Classic from Autoimmun Diagnostika GmbH and AID ELISpot Reader Software, Autoimmun Diagnostika). Student's *t*-test was performed in GraphPad Prism v8.0.1 software to statistically analyze the data.

Data availability

All data generated or analyzed during the study are included in this article.

Acknowledgments

This study was supported by the National Major Scientific and Technological Special Project for “Significant New Drug Development” (2018ZX09733002), the Key Research and Development Program of Hubei province (2020BCA062), and the National Natural Science Foundation of China (NSFC) (Grant No. 81972308). The National Natural Science Foundation of China (21473065 & 819723082), the 111 Project (B17019), the National Key Research and Development Program of China (2017YFA0505200).

References:

1. Green, M.R. & Sambrook, J. How to Win the Battle with RNase. *Cold Spring Harb Protoc*. **2019** (2019).
2. Eygeris, Y., Gupta, M., Kim, J. & Sahay, G. Chemistry of Lipid Nanoparticles for RNA Delivery. *Acc Chem. Res.* **55**, 2-12 (2022).
3. Wu, M.Z., Asahara, H., Tzertzinis, G. & Roy, B. Synthesis of low immunogenicity RNA with high-temperature in vitro transcription. *RNA*. **26**, 345-360 (2020).
4. Anderson, E.J. et al. Safety and Immunogenicity of SARS-CoV-2 mRNA-1273 Vaccine in Older Adults. *N Engl. J. Med*. **383**, 2427-2438 (2020).
5. Davalos, V., Blanco, S. & Esteller, M. SnapShot: Messenger RNA Modifications. *Cell* **174**, 498 (2018).
6. Gloge, F., Becker, A.H., Kramer, G. & Bukau, B. Co-translational mechanisms of protein maturation. *Curr. Opin. Struct. Biol*. **24**, 24-33 (2014).
7. Huber, S.M. et al. Formation and abundance of 5-hydroxymethylcytosine in RNA. *Chembiochem.* **16**, 752-755 (2015).
8. Fu, L. et al. Tet-mediated formation of 5-hydroxymethylcytosine in RNA. *J. Am. Chem. Soc*. **136**, 11582-11585 (2014).
9. Dimitrova, D.G., Teysset, L. & Carre, C. RNA 2'-O-Methylation (Nm) Modification in Human Diseases. *Genes (Basel)*. **10** (2019).
10. Dai, Q. et al. Nm-seq maps 2'-O-methylation sites in human mRNA with base precision. *Nat. Methods*. **14**, 695-698 (2017).
11. Boo, S.H. & Kim, Y.K. The emerging role of RNA modifications in the regulation of mRNA stability. *Exp. Mol. Med*. **52**, 400-408 (2020).
12. Dominissini, D. et al. The dynamic N(1)-methyladenosine methylome in eukaryotic messenger RNA. *Nature*. **530**, 441-446 (2016).
13. Wang, X. et al. N6-methyladenosine-dependent regulation of messenger RNA stability. *Nature*. **505**, 117-120 (2014).
14. Wang, X. et al. N(6)-methyladenosine Modulates Messenger RNA Translation Efficiency. *Cell* **161**, 1388-1399 (2015).
15. Cao, G., Li, H.B., Yin, Z. & Flavell, R.A. Recent advances in dynamic m6A RNA modification. *Open Biol.* **6**, 160003 (2016).
16. Yang, Y. et al. RNA 5-Methylcytosine Facilitates the Maternal-to-Zygotic Transition by Preventing Maternal mRNA Decay. *Mol. Cell*. **75**, 1188-1202 (2019).
17. Shi, H., Chai, P., Jia, R. & Fan, X. Novel insight into the regulatory roles of diverse RNA modifications: Re-defining the bridge between transcription and translation. *Mol. Cance.r* **19**, 78 (2020).
18. Yang, X. et al. 5-methylcytosine promotes mRNA export - NSUN2 as the methyltransferase and ALYREF as an m(5)C reader. *Cell Res.* **27**, 606-625 (2017).
19. Kurth, H.M. & Mochizuki, K. 2'-O-methylation stabilizes Piwi-associated small RNAs and ensures DNA elimination in Tetrahymena. *RNA*. **15**, 675-685 (2009).
20. Sproat, B.S., Lamond, A.I., Beijer, B., Neuner, P. & Ryder, U. Highly efficient chemical synthesis of 2'-O-methyloligoribonucleotides and tetrabiotinylated derivatives; novel probes that are resistant to degradation by RNA or DNA specific nucleases. *Nucleic. Acids. Res*. **17**, 3373-3386 (1989).
21. Byszewska, M., Smietanski, M., Purta, E. & Bujnicki, J.M. RNA methyltransferases involved in 5' cap biosynthesis. *Rna. Biol*. **11**, 1597-1607 (2014).
22. Kumar, S., Mapa, K. & Maiti, S. Understanding the effect of locked nucleic acid and 2'-O-methyl

modification on the hybridization thermodynamics of a miRNA-mRNA pair in the presence and absence of AfPiwi protein. *Biochemistry-Us.* **53**, 1607-1615 (2014).

23. Yildirim, I., Kierzek, E., Kierzek, R. & Schatz, G.C. Interplay of LNA and 2'-O-methyl RNA in the structure and thermodynamics of RNA hybrid systems: a molecular dynamics study using the revised AMBER force field and comparison with experimental results. *J. Phys. Chem. B.* **118**, 14177-14187 (2014).
24. Davis, F.F. & Allen, F.W. Ribonucleic Acids From Yeast Which Contain a Fifth Nucleotide. *J. Biol. Chem.* **227**, 907-915 (1957).
25. Kariko, K., Buckstein, M., Ni, H. & Weissman, D. Suppression of RNA recognition by Toll-like receptors: the impact of nucleoside modification and the evolutionary origin of RNA. *Immunity.* **23**, 165-175 (2005).
26. Kariko, K. et al. Incorporation of pseudouridine into mRNA yields superior nonimmunogenic vector with increased translational capacity and biological stability. *Mol. Ther.* **16**, 1833-1840 (2008).
27. Andries, O. et al. N(1)-methylpseudouridine-incorporated mRNA outperforms pseudouridine-incorporated mRNA by providing enhanced protein expression and reduced immunogenicity in mammalian cell lines and mice. *J. Control. Release.* **217**, 337-344 (2015).
28. Nance, K.D. & Meier, J.L. Modifications in an Emergency: The Role of N1-Methylpseudouridine in COVID-19 Vaccines. *ACS. Cent. Sci.* **7**, 748-756 (2021).
29. Conry, R.M. et al. Characterization of a messenger RNA polynucleotide vaccine vector. *Cancer. Res.* **55**, 1397-1400 (1995).
30. Schlake, T., Thess, A., Fotin-Mleczek, M. & Kallen, K.J. Developing mRNA-vaccine technologies. *RNA. Biol.* **9**, 1319-1330 (2012).
31. Kariko, K., Kuo, A. & Barnathan, E. Overexpression of urokinase receptor in mammalian cells following administration of the in vitro transcribed encoding mRNA. *Gene. Ther.* **6**, 1092-1100 (1999).
32. Sahin, U., Kariko, K. & Tureci, O. mRNA-based therapeutics--developing a new class of drugs. *Nat. Rev. Drug. Discov.* **13**, 759-780 (2014).
33. Pelletier, J., Kaplan, G., Racaniello, V.R. & Sonenberg, N. Cap-independent translation of poliovirus mRNA is conferred by sequence elements within the 5' noncoding region. *Mol. Cell. Biol.* **8**, 1103-1112 (1988).
34. Jang, S.K. & Wimmer, E. Cap-independent translation of encephalomyocarditis virus RNA: structural elements of the internal ribosomal entry site and involvement of a cellular 57-kD RNA-binding protein. *Genes. Dev.* **4**, 1560-1572 (1990).
35. Macejak, D.G. & Sarnow, P. Internal initiation of translation mediated by the 5' leader of a cellular mRNA. *Nature.* **353**, 90-94 (1991).
36. Pyronnet, S., Pradayrol, L. & Sonenberg, N. A cell cycle-dependent internal ribosome entry site. *Mol. Cell.* **5**, 607-616 (2000).
37. Teo, S.P. Review of COVID-19 mRNA Vaccines: BNT162b2 and mRNA-1273. *J. Pharm. Pract.* 1292474482 (2021).
38. Bangham, A.D. & Horne, R.W. Negative Staining Of Phospholipids And Their Structural Modification By Surface-Active Agents As Observed In The Electron Microscope. *J. Mol. Biol.* **8**, 660-668 (1964).
39. Bangham, A.D., Horne, R.W., Glauert, A.M., Dingle, J.T. & Lucy, J.A. Action of saponin on biological cell membranes. *Nature.* **196**, 952-955 (1962).
40. Barenholz, Y. Doxil(R)--the first FDA-approved nano-drug: lessons learned. *J. Control Release.* **160**, 117-134 (2012).
41. Saw, P.E. & Song, E.W. siRNA therapeutics: a clinical reality. *Sci China Life. SCI* **63**, 485-500 (2020).

42. Cho, H.Y., Chuang, T.H. & Wu, S.N. Effective Perturbations on the Amplitude and Hysteresis of Erg-Mediated Potassium Current Caused by 1-Octylnonyl 8-[(2-hydroxyethyl)[6-oxo-6(undecyloxy)hexyl]amino]-octanoate (SM-102), a Cationic Lipid. *Biomedicines*. **9** (2021).
43. Crommelin, D., Anchordoquy, T.J., Volkin, D.B., Jiskoot, W. & Mastrobattista, E. Addressing the Cold Reality of mRNA Vaccine Stability. *J. Pharm. Sci*. **110**, 997-1001 (2021).
44. Maugeri, M. et al. Linkage between endosomal escape of LNP-mRNA and loading into EVs for transport to other cells. *Nat. Commun*. **10**, 4333 (2019).
45. To, K. & Cho, W. An overview of rational design of mRNA-based therapeutics and vaccines. *Expert. Opin. Drug Discov*. **16**, 1307-1317 (2021).
46. Hassett, K.J. et al. Optimization of Lipid Nanoparticles for Intramuscular Administration of mRNA Vaccines. *Mol. Ther. Nucleic Acids.* **15**, 1-11 (2019).
47. Saadeldin, M.K., Abdel-Aziz, A.K. & Abdellatif, A. Dendritic cell vaccine immunotherapy; the beginning of the end of cancer and COVID-19. A hypothesis. *Med. Hypotheses*. **146**, 110365 (2021).
48. Schuler-Thurner, B. et al. Immunotherapy of uveal melanoma: vaccination against cancer. Multicenter adjuvant phase 3 vaccination study using dendritic cells laden with tumor RNA for large newly diagnosed uveal melanoma. *Ophthalmologe.* **112**, 1017-1021 (2015).
49. McNamara, M.A., Nair, S.K. & Holl, E.K. RNA-Based Vaccines in Cancer Immunotherapy. *J. Immunol. Res*. **2015**, 794528 (2015).
50. Pallesen, J. et al. Immunogenicity and structures of a rationally designed prefusion MERS-CoV spike antigen. *Proc. Natl. Acad. Sci. USA.* **114**, E7348-E7357 (2017).
51. Schlee, M. & Hartmann, G. Discriminating self from non-self in nucleic acid sensing. *Nat. Rev. Immunol.* **16**, 566-580 (2016).
52. August, A. et al. A phase 1 trial of lipid-encapsulated mRNA encoding a monoclonal antibody with neutralizing activity against Chikungunya virus. *Nat. Med.* **27**, 2224-2233 (2021).
53. Nicolas, J.F. & Guy, B. Intradermal, epidermal and transcutaneous vaccination: from immunology to clinical practice. *Expert Rev. Vaccines.* **7**, 1201-1214 (2008).
54. Vogel, A.B. et al. BNT162b vaccines protect rhesus macaques from SARS-CoV-2. *Nature*. **592**, 283-289 (2021).
55. Pardi, N., Hogan, M.J., Porter, F.W. & Weissman, D. mRNA vaccines - a new era in vaccinology. *Nat. Rev. Drug Discov*. **17**, 261-279 (2018).
56. Pallesen, J. et al. Immunogenicity and structures of a rationally designed prefusion MERS-CoV spike antigen. *Proc. Natl. Acad. Sci. USA.* **114**, E7348-E7357 (2017).
57. Muench, L.R.H. A Simple Method Of Estimating Fifty Per Cent Endpoints. *American Journal of Epidemiology*. **27**, 493-497 (1938).
58. Shi, G.L. et al. Construction of a new oncolytic virus oHSV2hGM-CSF and its anti-tumor effects. *Zhonghua Zhong Liu Za Zhi*. **34**, 89-95 (2012).